metals

MDPI

Article

Heat Dissipation of Open-Cell-Type Aluminum Foams Manufactured by Replication-Casting Process

Jongmin Kim, Taekyu Ha, Youngki Lee, Byungil Kang and Youngjig Kim *

Department of Advanced Materials Science and Engineering, Sungkyunkwan University, 2066 Seobu-ro, Jangan-gu, Suwon 16419, Republic of Korea; win95win95@skku.edu (J.K.); taekyu@skku.edu (T.H.); galeans@skku.edu (Y.L.); subs39th@skku.edu (B.K.)
* Correspondence: yjk1122@skku.edu

Abstract: Open-cell-type aluminum foam demonstrates excellent heat dissipation owing to interconnected pores. In this study, open-cell-type aluminum foams with various pore sizes and porosities were fabricated using the replication-casting process, which is a relatively simple process. The porosity of the manufactured foams ranged from approximately 55% to 62%. To assess the heat dissipation of the manufactured foams, an air-cooling system was designed. The device could pass a controlled amount of air through the connected pores, simultaneously measuring pressure drop ΔP and temperature changes. It was confirmed that the open-cell-type aluminum foams exhibited a very high cooling rate in the initial cooling phase, and the thermal behavior is influenced by structural characteristics. At a porosity of 62%, the initial maximum cooling rate was measured to be 1.41 °C/s for a pore size of 0.7~1.0 mm, and it was observed to significantly increase to 3.82 °C/s for a pore size of 2.8~3.4 mm. Furthermore, for the same pore size, an increase in porosity resulted in an increase in the initial cooling rate. Lager pore sizes and higher porosities led to lower pressure drop ΔP and improved airflow, enhancing the cooling efficiency of open-cell-type aluminum foams.

Keywords: aluminum foam; open-cell type; replication casting; thermal property; heat dissipation

check for updates

Citation: Kim, J.; Ha, T.; Lee, Y.; Kang, B.; Kim, Y. Heat Dissipation of Open-Cell-Type Aluminum Foams Manufactured by Replication-Casting Process. *Metals* **2024**, *14*, 206. https://doi.org/10.3390/met14020206

Academic Editor: Bin Han

Received: 4 January 2024
Revised: 1 February 2024
Accepted: 6 February 2024
Published: 7 February 2024

Copyright: © 2024 by the authors. Licensee MDPI, Basel, Switzerland. This article is an open access article distributed under the terms and conditions of the Creative Commons Attribution (CC BY) license (https://creativecommons.org/licenses/by/4.0/).

1. Introduction

Aluminum foam contains numerous pores within the material, which are expressed as the porosity or relative density of the foam. There are two types depending on the internal pore structure of the aluminum foams. One is the closed-cell type in which the internal pores exist independently; the other is the open-cell type with interconnected internal pores [1–3]. In the case of open-cell-type aluminum foam, liquid and gas can flow through the empty spaces between the cells, providing excellent heat and mass transport [4,5].

The porous structure of metal foams can exhibit a variety of characteristics depending on the structural conditions, such as lightweight, specific surface area, high energy absorption, and heat resistant/dissipation characteristics [1–3,6,7]. Moreover, the advantage is that it can be applied to one product by combining two or more characteristics [8]. These excellent properties of aluminum foams make them applicable in various industrial fields like aerospace, automotive, railway, etc. [7–9]. However, most of the applications of aluminum foams currently used are in terms of lightweight, energy-absorbing, and heat-resistant products. These products are generally made of closed-cell type aluminum foams because they are relatively simple to manufacture and can be mass-produced. On the other hand, even though open-cell-type aluminum foams can be applied to various fields based on heat and mass transport with interconnected pores [10–12], there is a limit to use in many industrial fields due to the following conventional manufacturing processes.

There are several methods for producing open-cell-type aluminum foams, including investment casting, vapor deposition, sintering, etc. In the case of investment casting, open-cell-type aluminum foams can be manufactured using a pattern of a desired shape [13].

Typically, a polyurethane foam pattern is used, and a mold with a porous structure is manufactured by filling the interior of the pattern with a refractory material like ceramic slurry [13,14]. However, this process is complex and time-consuming due to the numerous steps involved. The vapor deposition process is another method that utilizes a polymer template, with metal precursors deposited on the template to create open-cell-type aluminum foam [15]. While this method allows for the fabrication of foams with high porosity, approximately 97%, there are drawbacks. The deposition process is unsuitable for mass production due to its slow speed, and the equipment and process stages incur high production costs. Sintering, a process involving the compaction of a solid mass with metal powders through compression or heating, is also utilized in the production of open-cell-type aluminum foams [16,17]. Various variables such as sintering temperature, time, pressure, and atmosphere must be controlled to influence structural characteristics like density and porosity. However, while useful for manufacturing open-cell-type aluminum foams with high porosity exceeding 80%, lower porosities may lead to trapped spacers causing contamination and corrosion [16,18]. The centrifugal casting process has the advantage of using NaCl spherical particles to manufacture open-cell-type foams with the desired pore size [19]. A. Sánchez et al. utilized a centrifugal casting device to inject a melt of Zn-22Al-2Cu into a stainless-steel cylinder containing NaCl particles, and the pressure generated by rotation filled the spaces between NaCl particles. Through this process, open-cell-type foams with three different pore sizes were produced. However, this process has limitations in terms of manufacturing sample size due to the constraints of the processing technique. In addition to the aforementioned methods, 3D printing techniques have recently been actively studied for open-cell-type aluminum foam production [20,21]. This method allows for the design of foams with diverse pore shapes and sizes, but it comes with disadvantages, such as long manufacturing times, high production costs, and significant initial investments [21]. Despite the excellent properties of open-cell-type aluminum foams, their application is limited to certain industries due to these drawbacks. Therefore, for practical and widespread use, there is a need to develop cost-effective and simple processes for producing open-cell-type aluminum foams.

For the practical application of open-cell-type metal foams, a systematic analysis of characteristic evaluation needs to accompany the manufacturing process. In the case of open-cell-type metal foams, the easy passage of fluid through interconnected pores allows for efficient dissipation of internal heat to the external. In this process, there are two significant thermal behaviors [22,23]. Firstly, forced convection induces the flow of fluid through interconnected pores, leading the foam to release heat to the external. Secondly, through the heat conduction within the foam, heat moves from higher to lower temperatures. Particularly, aluminum alloys with high thermal conductivity can rapidly conduct heat across the entire foam, enhancing heat dissipation. Additionally, heat radiation through the metal cell walls can occur, but this is reported to have an impact primarily in very high temperature ranges [24]. Many researchers have conducted studies on the thermal properties of open-cell-type metal foams. Mauro Bracconi et al. investigated heat transfer in the solid matrix of open-cell-type metal foams using 3D numerical simulation and performed an analysis of the correlation between porosity and heat transfer [25]. However, the results are limited to forms with high porosity (>90%) produced through additive manufacturing techniques. Zhengwei Nie et al. analyzed the pressure drop ΔP in open-cell-type metal foams based on porosity using CFD simulations and compared the results with theoretical predictions [26]. Nevertheless, they observed a deviation of approximately 20% compared to theoretical predictions. Parham Poureslami et al. conducted an investigation on the pressure drop ΔP and thermal conductivity of open-cell-type metal foams based on pore size using the multi-relaxation-time lattice Boltzmann method (MRT-LBM) [27]. They confirmed that as the pore size decreases, both the pressure drop ΔP and the thermal conductivity increase. However, all three studies mentioned are simulation results based on the ideal geometric model of metal foams. In recent research, numerous investigations on the thermal behavior of open-cell-type metal foams have been conducted, with the

majority focusing on predictions through CFD simulations and comparison with theoretical results [25–30]. Further research is needed to investigate the correlation between pressure drop ΔP and cooling performance (heat dissipation) based on the structural features of open-cell-type metal foams when fluid passes through interconnected pores. Conducting experimental studies in these aspects is desirable.

In a previous study, open-cell-type aluminum foams were manufactured using A356 and ADC12 commercial aluminum alloys, and the thermal properties according to structural conditions were evaluated using the hot plate method [31]. Additionally, within the foams under the same structural conditions, variations in thermal properties were observed depending on the alloy type, attributed to differences in thermal conductivity due to variations in chemical composition. However, this method is somewhat static as an experimental approach that measures the changing temperature simply by applying heat to the foams.

In this work, we focus on the replication-casting process, a relatively simple method capable of fabricating open-cell-type aluminum foams using molten aluminum alloy and a space holder. Alongside introducing this straightforward process, which enables control over pore size and porosity [32,33], the heat dissipation of the foams was evaluated to understand their relationship with structural characteristics affecting heat and mass transport. Due to the absence of international test standards for evaluating the heat dissipation of open-cell-type aluminum foams, an air-cooling system was designed to induce forced convection within the foams. Through this device, the differences in the pressure drop ΔP and the temperature variation resulting from injecting the same airflow rate into the foams were compared and analyzed based on structural conditions. The results also include variations observed when the airflow rate is varied. This method overcomes the limitations of thermal evaluation in previous work and is suitable for assessing cooling performance according to structural conditions by utilizing the advantages of open-cell-type aluminum foams.

2. Experimental Procedure

2.1. Manufacturing Method of Open-Cell-Type Aluminum Foam by Replication Casting

The manufacturing method of open-cell-type aluminum foam by replication casting is divided into the following three steps: (1) preparation and ramming of the space holder, (2) infiltration of Al melts, and (3) dissolution, as illustrated in Figure 1. Molten aluminum alloy is cast into the spaces between space holders in the container, and the space holders are removed after the melts completely solidify. However, during these stages, such as setting up the space holders and pouring the melts, certain problems arise. For example, during the molten aluminum alloy infiltration process, issues such as space holders floating can arise due to differences in density and turbulence in the melts. Therefore, this paper will address important factors and precautions at each stage of the process in detail.

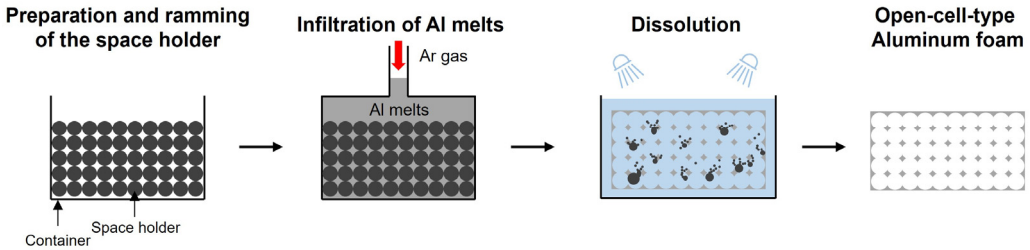

Figure 1. Manufacturing method of open-cell-type aluminum foams by replication-casting process.

2.1.1. Preparation and Ramming of the Space Holder

The space holder plays a crucial role in forming the pores of the final product, so the structural features, such as pore size and porosity, are determined by the size and stacked conditions of the space holder. The space holders are made using Na_2CO_3 powder with a purity of 99.8% because they must be easily removed after filling Al melts between the space holders. Additionally, they should have a high melting temperature because they come into

contact with the melts of more than 700 °C (melting temperature of Na_2CO_3: 851 °C). The space holders were prepared for manufacturing foams as following steps. First, Na_2CO_3 powder was melted in a furnace at 900 °C for 1 h and solidified to prepare a Na_2CO_3 ingot. Next, the Na_2CO_3 ingot was crushed and sieved by size (2.8~3.4 mm, 1.0~2.0 mm, 0.7~1.0 mm). The space holders were angular in shape due to a crushing process. Finally, the space holders for each size were stacked in a container. In this process, the stacking density of the space holders is a factor determining the porosity of the aluminum foam, so the space holders were stacked by varying the number of ramming counts. For instance, with two rammings, 300 g of space holders are stacked twice in increments of 150 g, while with five rammings, 60 g of space holders are stacked five times. Additionally, two SiC filters of 30 ppi were installed between the space holders stacked in the container; the bottom one was to provide space for residual gas inside, and the top one was to prevent the space holders from floating during infiltration of aluminum alloy melts. In this stage, increasing the number of ramming counts leads to a higher stacking density of the space holder and an expected increase in the porosity of the foam.

2.1.2. Infiltration of Al Melts

It is a stage of filling the empty spaces between the space holders stacked according to the desired size and ramming counts in the container by casting molten aluminum alloy. The chamber used for manufacturing open-cell-type aluminum foams by replication casting was designed in this work, as shown in Figure 2. The chamber, connected to a gas pressurizing device for filling molten aluminum alloy and a vacuum pump to remove the internal gas before filling, was capable of being heated to 1200 °C in an electric furnace. The container in which the space holders were stacked in the first stage (Preparation and ramming of the space holder) was mounted in the chamber. At this stage, proper casting parameters, including space holder preheating, melt temperature, and gas pressure, are essential for effective infiltration without leaving empty spaces or trapped space holders. When infiltrating aluminum alloy melts, the alloy used in the experiment was A356 aluminum alloy, and the chemical composition is shown in Table 1. The casting parameters were set as follows: preheating temperature of the space holder at 600 °C, melts temperature at 730 °C, and gas pressure at 2 bar. As a result of infiltrating 1 kg of A356 aluminum alloy melts with the specified casting parameters, the melts were successfully charged between the space holders under all stacking conditions. Figure 3a shows the sample stacked 5 times with space holders of 2.8~3.4 mm. The foam was positioned between the filters and wrapped with kaowool paper for tight fixation.

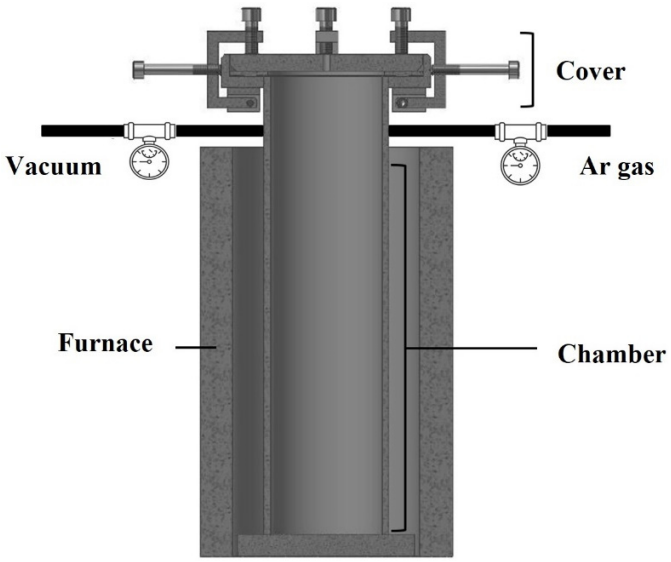

Figure 2. Chamber of replication casting in this work.

Table 1. Chemical composition of A356 aluminum alloy.

Elements	Si	Fe	Cu	Mn	Mg	Zn	Ti	Al
wt.%	7.08	0.20	0.08	0.05	0.29	0.02	0.12	bal.



(**a**) (**b**) (**c**)

Figure 3. Open-cell-type aluminum foam manufactured by replication casting: (**a**) before cutting, (**b**) before dissolution, and (**c**) after dissolution.

2.1.3. Dissolution

The cross-sectional area of the sample is shown in Figure 3b after cutting the upper and lower filters through electric discharge processing. The space holders were located inside the sample, and it was immersed in water to remove the space holders. Since optimal Na_2CO_3 solubility occurs at a water temperature of 35 to 40 °C [34], it was dissolved at that temperature, and the efficiency can be enhanced by stirring the water or ultrasonic injection. After dissolution, the pores replicated the same shape and size as the space holders, as shown in Figure 3c.

2.2. Measurement Method

2.2.1. Porosity

Open-cell-type aluminum foams, composed of numerous inter pores, are lighter compared to a bulk material without pores, and this weight difference varies with the volume of the pores. Relative density ε is a ratio representing the density of the foam relative to the density of the bulk material without pores. In this work, the open-cell-type aluminum foams with the space holder sizes (2.8~3.4 mm, 1.0~2.0 mm, and 0.7~1.0 mm) and ramming counts (2 times and 5 times) were prepared through the replication-casting process as shown in Figure 4. When the volume of a foam and a bulk material are equal, the relative density of the foam is described as presented in Equation (1). To calculate the relative density of the foams according to the structural conditions, the open-cell-type aluminum foams and the bulk material were prepared in dimensions of $47.5 \times 47.5 \times 42$ mm^3. The weights of the foams m_f and the bulk material m_b were measured, and the relative density was calculated using Equation (1).

$$\varepsilon = \frac{m_f}{m_b} \quad (1)$$

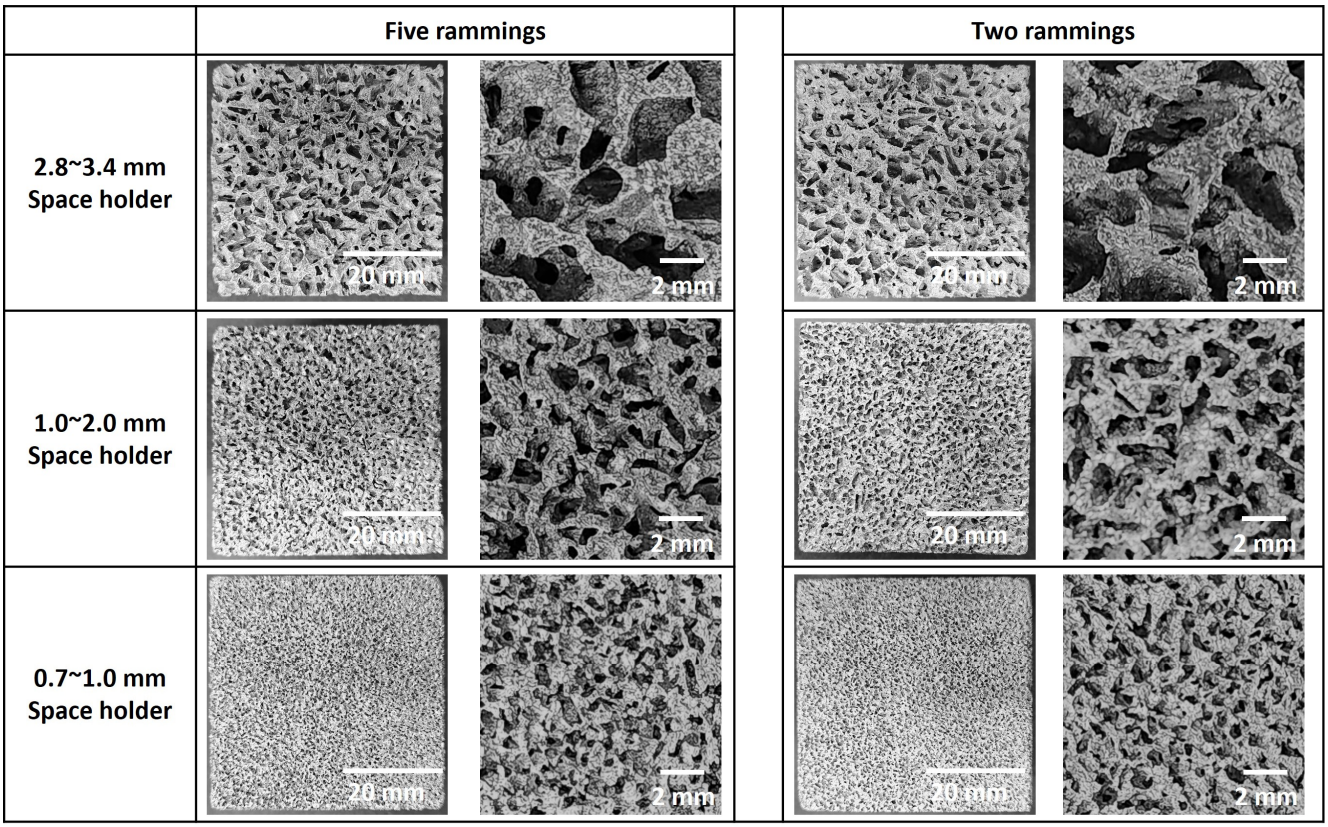

Figure 4. A356 open-cell-type aluminum foams manufactured by replication-casting process.

Porosity π refers to the fraction of the pore volume over the total volume, indicating the number of internal pores in the foams. In this study, the comparison of the thermal properties with the structural conditions was based on porosity and pore size. The porosity of the foams was calculated using Equation (2), employing the relative density of the foams for each structural condition.

$$\pi = \left(\frac{m_b - m_f}{m_b}\right) \times 100 = (1 - \varepsilon) \times 100 \quad (2)$$

2.2.2. Cell Wall Thickness

In the case of cell walls coexisting with pores within foams, the thickness can vary depending on the pore size and porosity. For the open-cell-type aluminum foams manufactured in this study, the shape of the pores is irregular polyhedrons. Calculating the cell wall thickness within the foams through mathematical calculations has limitations, as the structure deviates from an ideal geometric model. Therefore, as shown in Figure 5, the thickness of the cell walls present above five horizontal lines and two diagonals on the surface of the foams was measured, and this measurement was conducted using the Image Pro Plus V6.0 program.

2.3. Thermal Properties Evaluation: Air-Cooling System

Since the pores in open-cell-type aluminum foams are interconnected with each other, both liquid and gas can flow through them. The heat of open-cell-type aluminum foams can be dissipated by heat- and mass-transport characteristics, and the cooling rate varies with the pore size and porosity. Therefore, in this work, an air-cooling system for open-cell-type aluminum foams was designed, as shown in Figure 6. A holder capable of fixing the sample was mounted in the center part based on a pipe through which the fluid could flow. The sample is heated by a coiled band heater, and Teflon gaskets were inserted between the pipe and the fixing part of the sample to prevent heat transport from the band heater to the pipe.

Based on the pipe, it is connected to a mass flow controller (MS3400V, Linetech, Daejeon, Republic of Korea) on one side to allow the sample to cool by airflow. Thermocouples capable of measuring the temperature of the sample were connected to a data logger (GL240, Graphtec, Shinano, Japan), and the airflow was determined by measuring the pressure at the inlet and outlet with a differential pressure sensor (MP112, KIMO, Montpon, France). As can be seen in Figure 6, five thermocouples were inserted into the device to measure the temperature in real-time. For CH1 and CH5, these present the ambient temperature at the inlet and outlet where air enters. CH2, CH3, and CH4 represent the temperature of the sample. CH2 is the point where the sample first contacts the air, CH3 is the middle point, and CH4 is the point where the air exits.

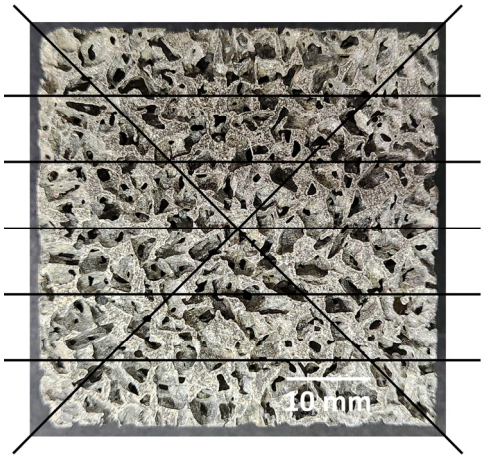

Figure 5. The baseline for measuring the cell wall thickness of open-cell-type aluminum foam.

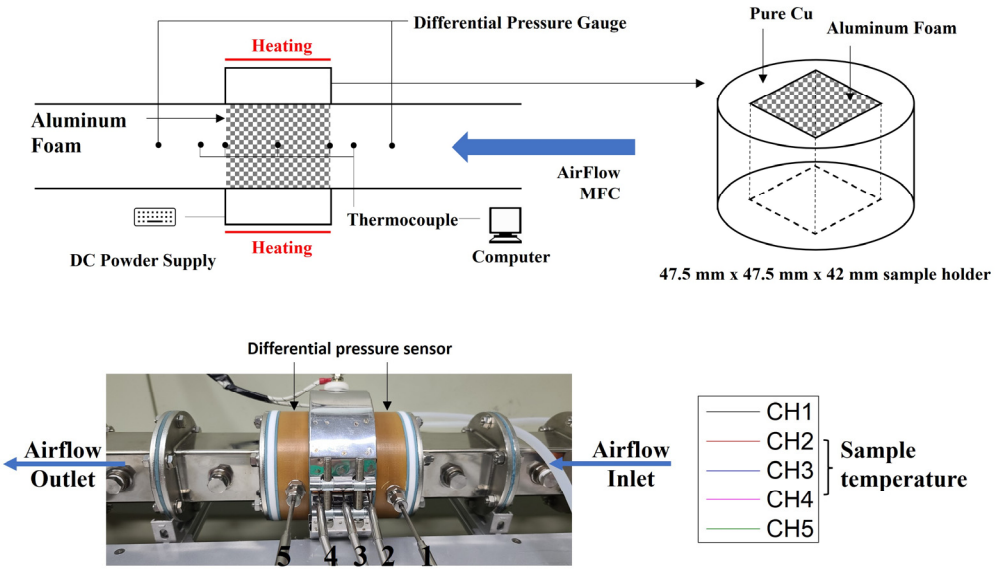

Figure 6. Air-cooling system for evaluating heat dissipation of open-cell-type aluminum foam.

For each sample manufactured (47.5 × 47.5 × 42 mm) using the replication-casting process, the same electrical energy of 22.4 V, 1.5 A was applied to heat the samples with the band heater for 4 h, and then volumetric airflow rates of 100 LPM and 50 LPM were injected to cool the samples. In the experimental process, temperature changes in the samples and the differential pressure between the inlet and the outlet were measured to evaluate the heat-dissipation ability with airflow through the samples corresponding to structural conditions of the open-cell-type aluminum foams.

3. Results and Discussion

3.1. Porosity

The relative density and porosity of the open-cell-type aluminum foams manufactured through replication-casting process are shown in Table 2. For an equal number of ramming counts, the porosity was approximately 55% with two rammings and about 62% with five rammings. It was confirmed that there is no significant difference in porosity depending on the size of the space holder. When the same size of space holder was stacked, the porosity increased by an average of 11.3% as the number of ramming counts increased from two to five. The pores inside the foams were formed by removing the space holders. Therefore, as the number of ramming counts increases, the density of the space holder per unit volume in the container increases, leading to an increase in the porosity of the open-cell-type aluminum foams. Through the process of manufacturing the foams and measuring porosity, it was verified that porosity could be controlled by the number of ramming counts, and pore size could be determined by the size of the space holder.

Table 2. Porosity and pressure drop of open-cell-type aluminum foams.

Ramming Count	Space Holder Size (mm)	Relative Density ε	Porosity π (%)	Average Cell Wall Thickness (mm)	ΔP, 100 LPM (mbar)	ΔP, 50 LPM (mbar)
5	2.8~3.4	0.373	62.7	1.76	61	15
5	1.0~2.0	0.381	61.9	0.88	80	25
5	0.7~1.0	0.388	61.2	0.22	108	34
2	2.8~3.4	0.441	55.9	2.03	70	18
2	1.0~2.0	0.447	55.3	1.01	89	28
2	0.7~1.0	0.452	54.8	0.26	119	37

3.2. Cell Wall Thickness

Figure 7 shows the measured values of cell wall thickness for the open-cell-type aluminum foams under the structural conditions, and the respective average values are presented in Table 2 and Figure 7. For the foams with a pore size of 2.8~3.4 mm, the average cell wall thickness decreased from 2.03 mm to 1.76 mm as the porosity increased from 55.9% to 62.7%. This result can be attributed to an increase in the volume of the space holder per unit volume, even with the use of the same-sized space holder, leading to a decrease in the available space for aluminum alloy filling. This trend was also observed under conditions with pore sizes of 1.0~2.0 mm and 0.7~1.0 mm, where the average cell wall thickness decreased by approximately 13.6% as the porosity increased from about 55% to 62%.

In the case of the foams with similar porosity levels, under a porosity of about 62%, as the pore size decreased to 2.8~3.4 mm, 1.0~2.0 mm, and 0.7~1.0 mm, the average cell size decreased significantly to 1.76 mm, 0.88 mm, and 0.22 mm. This is because, with a decrease in space holder size, the empty space for filling aluminum alloy melts between the particles becomes narrower. As a result, the average cell wall thickness decreases with an increase in porosity and a decrease in pore size, particularly exhibiting a substantial difference in average cell wall thickness with varying pore sizes.

3.3. Pressure Drop ΔP

Open-cell-type aluminum foams allow fluid to flow through internally interconnected pores, and the degree of fluid flow can vary depending on the structural conditions, such as pore size and porosity. In this study, the air-cooling system was utilized to assess the fluidity of air within the foams under different conditions. Subsequently, the heat-dissipation ability was comparatively analyzed using temperature changes and fluidity data of the foams obtained from the air-cooling system.

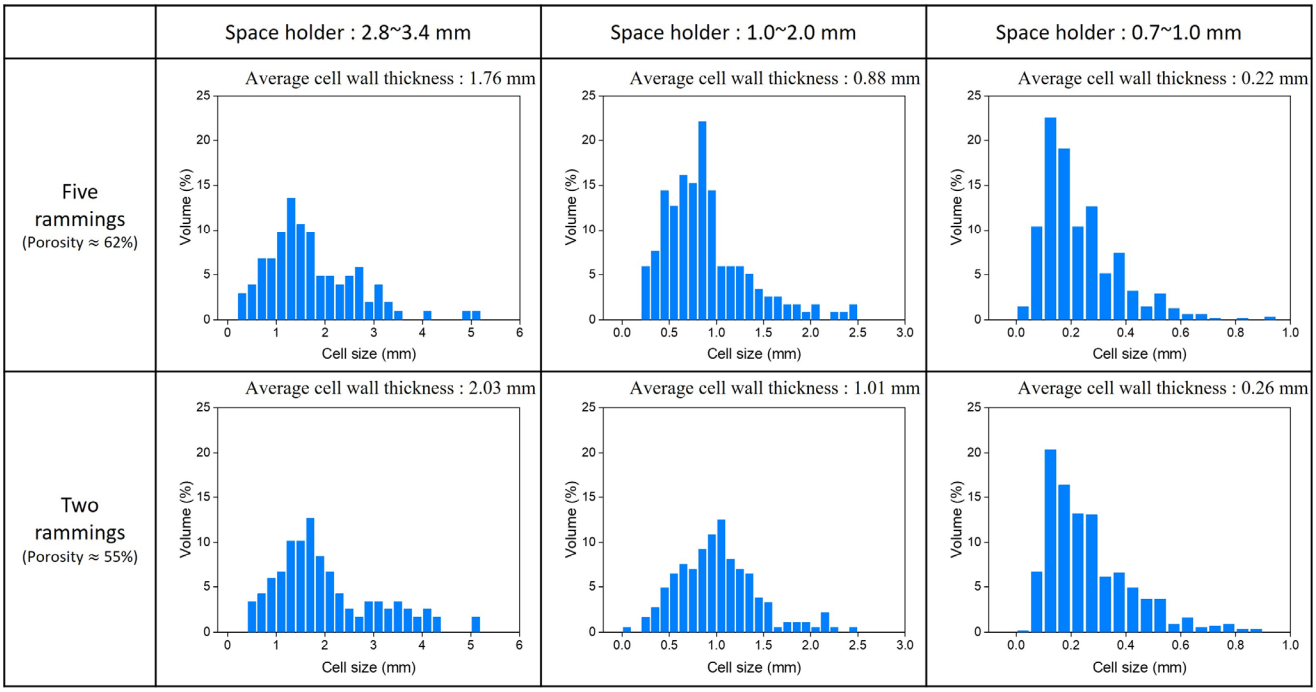

Figure 7. The cell wall thickness of open-cell-type aluminum foams with structural conditions.

Pressure drop ΔP means the difference in pressure between the air inlet and outlet, and the flow of air is better when the pressure drop is lower for the same amount of air injection. The pressure drop ΔP according to pore size and porosity, with airflow rates of 100 LPM and 50 LPM, is represented in Table 2 and Figure 8. At an airflow rate of 100 LPM, it was observed that, as the pore size decreased from 2.8 to 3.4 mm to 0.7 to 1.0 mm under the same condition of ramming counts, the pressure drop ΔP increased by more than 70%. When the porosity is at a similar level, a reduction in pore size results in a greater number of cell walls within the foam, and the cell wall thickness decreases. Numerous cells and cell walls become intricately entangled, forming a more complex structure, which makes fluid flow within the foam more challenging. The obtained results are in good agreement with the simulation data of the literature [27]. They reported simulation results indicating that as the pore size decreases, the permeability decreases. The decrease in permeability in foams means an increase in flow resistance of the air flowing through the pores, indicating an increase in pressure drop ΔP. In the case of the same pore size of 2.8~3.4 mm, it was measured that the pressure drop ΔP increased by approximately 15%, from 61 mbar to 70 mbar, as the porosity decreased. Even with the same pore size, as the pore volume per unit volume decreases, the cell thickness increases, resulting in an increase in pressure drop ΔP due to a reduction in the pathway available for airflow.

3.4. Heat Dissipation

The same energy (22.4 V, 1.5 A) was applied to the band heater for heating the foams, taking 4 h for the temperature change to stabilize. The stabilization temperature was about 99 °C to 100 °C, with no significant difference observed based on the structural conditions of the samples, as shown in Figure 9. CH2, CH3, and CH4 represent the temperature of the samples, and CH1 and CH5 indicate the ambient temperature based on the sample. When there is no airflow within the foams, and they are insulated from the outside, the stabilization temperature of the samples is the same.

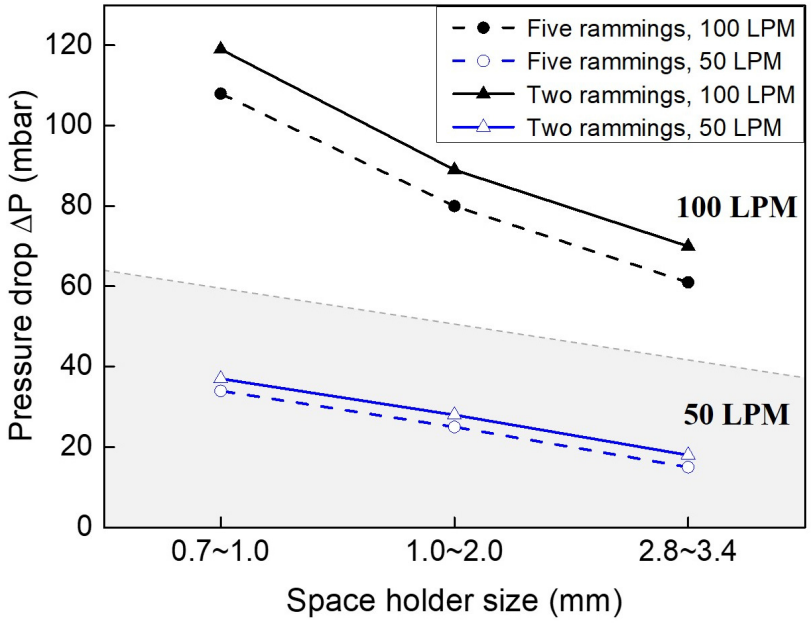

Figure 8. Pressure drop ΔP of the open-cell-type aluminum foams with structural conditions.

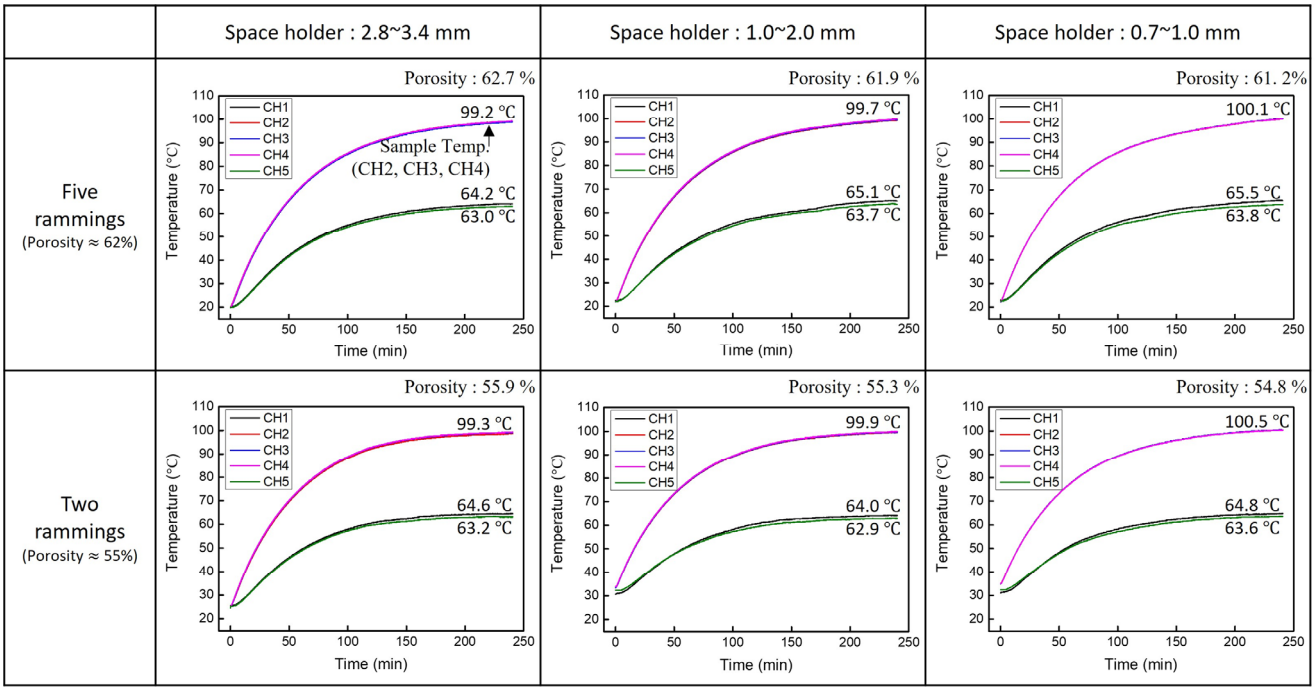

Figure 9. Temperature of the open-cell-type aluminum foams while heating by air-cooling system.

Figure 10 shows the temperature of the samples (five rammings) during air cooling with a flow rate of 100 LPM. After air injection, the temperature rapidly decreased, and the final stabilization temperature was measured at about 30 to 40 °C depending on the position after 1 h. The slope of the cooling temperature graphs varies with pore size, so to confirm this more clearly, it is converted into the graphs of cooling rate and shown in Figure 11, and the average cooling rate for each time interval is represented.

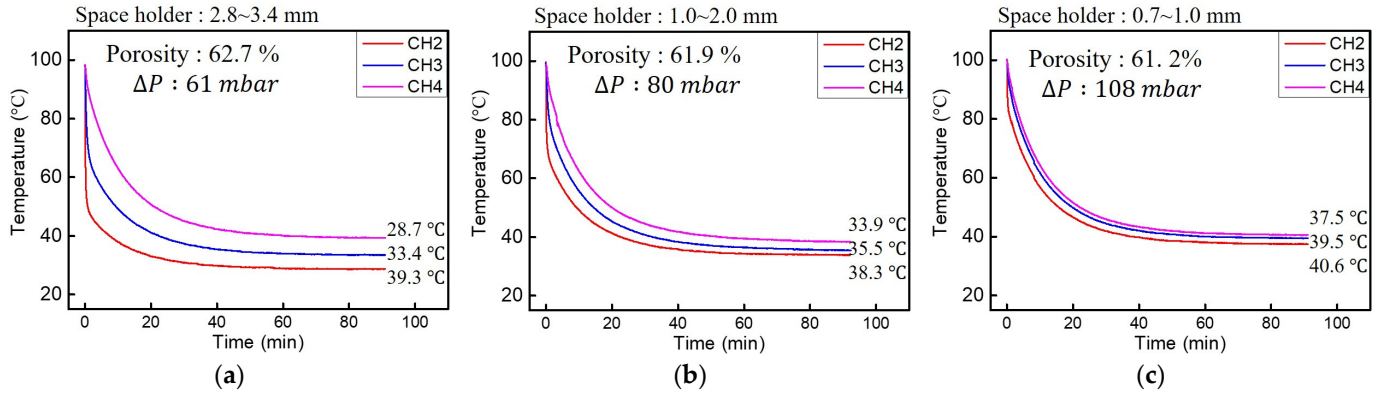

Figure 10. Temperature of the open-cell-type aluminum foams (five rammings) while cooling by air-cooling system—100 LPM: (**a**) 2.8~3.4 mm space holder; (**b**) 1.0~2.0 mm space holder; (**c**) 0.7~1.0 mm space holder.

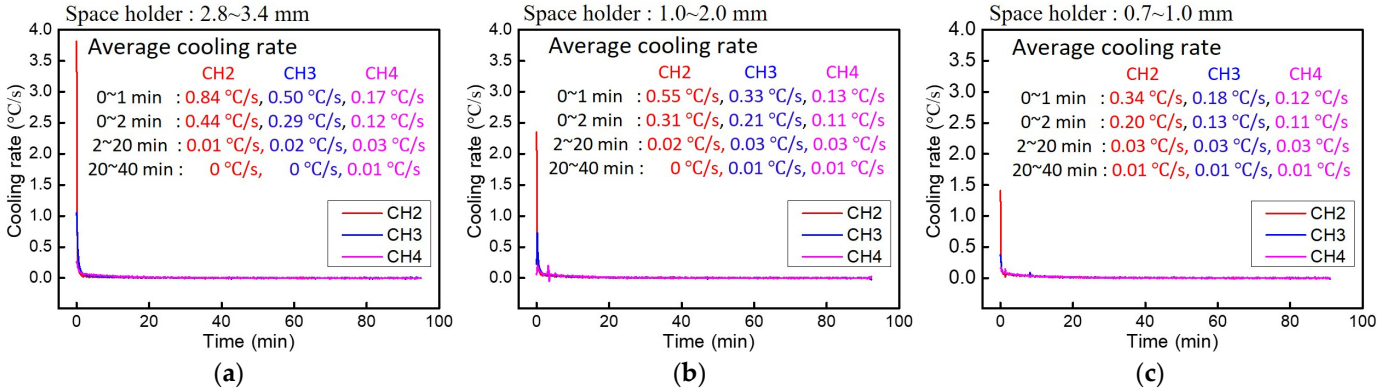

Figure 11. Cooling rate of the open-cell-type aluminum foams (five rammings) while cooling by air-cooling system—100 LPM: (**a**) 2.8~3.4 mm space holder; (**b**) 1.0~2.0 mm space holder; (**c**) 0.7~1.0 mm space holder.

As depicted in Figures 10 and 11, the stabilization temperature is similar among the samples, but the initial cooling rate is significantly different. In the case of the foam with a pore size of 2.8~3.4 mm, as shown in Figure 11, the average cooling rate from 0 to 1 min in CH2 is 0.84 °C/s. As the pore sizes decreased to 1.0~2.0 mm and 0.7~1.0 mm, the average cooling rates were measured at 0.55 °C/s and 0.34 °C/s, respectively. Additionally, the average cooling rates from 0 to 2 min in CH2 decreased to 0.44 °C/s, 0.31 °C/s, and 0.20 °C/s as the pore sizes decreased to 2.8~3.4 mm, 1.0~2.0, and 0.7~1.0 mm, respectively. The results indicate that structural conditions in open-cell-type aluminum foams significantly influence the cooling performance of the foams. In all foams, the cooling rate is very fast during the initial 0 to 2 min, followed by a rapid decrease in cooling rate. However, it was observed that the initial cooling rate varies significantly based on the structural conditions. Therefore, for an accurate comparison, it is necessary to closely analyze the interval of 0 to 2 min where the differences in cooling rates are noticeable.

Figure 12 shows the cooling rate of the foams (five rammings) during the first 2 min of cooling using the air-cooling system with 100 LPM. Each graph represents the maximum cooling rate within the specified conditions. Comparing the maximum cooling rates of the open-cell-type aluminum foams in CH2 under different conditions, it is remarkably fast at 3.82 °C/s for the foam with a pore size of 2.8~3.4 mm, while the maximum cooling rates decrease to 2.35 °C/s and 1.41 °C/s as the pore sizes decrease to 1.0~2.0 mm and 0.7~1.0 mm, respectively. The maximum cooling rate of the foam with a pore size of 1.0~2.0 mm decreased by about 38.5% compared to the foam with a pore size of 2.8~3.4 mm, and for a pore size of 0.7~1.0 mm, the decrease was 40% compared to the foam with a

pore size of 1.0~2.0 mm. These results indicate that as the pore size within open-cell-type aluminum foams decreases under similar porosity levels, the cooling performance diminishes, signifying a reduction in heat-dissipation efficiency. Generally, as the pore size of open-cell-type aluminum foams decreases, the surface area to volume ratio of pores per unit volume increases. Richardson et al. and Liu et al. reported the relationship between specific surface area S_v per unit volume and pore sizes of porous materials as Equation (3) [35,36].

$$S_v = \frac{4\pi}{d_p(1-\pi)} \tag{3}$$

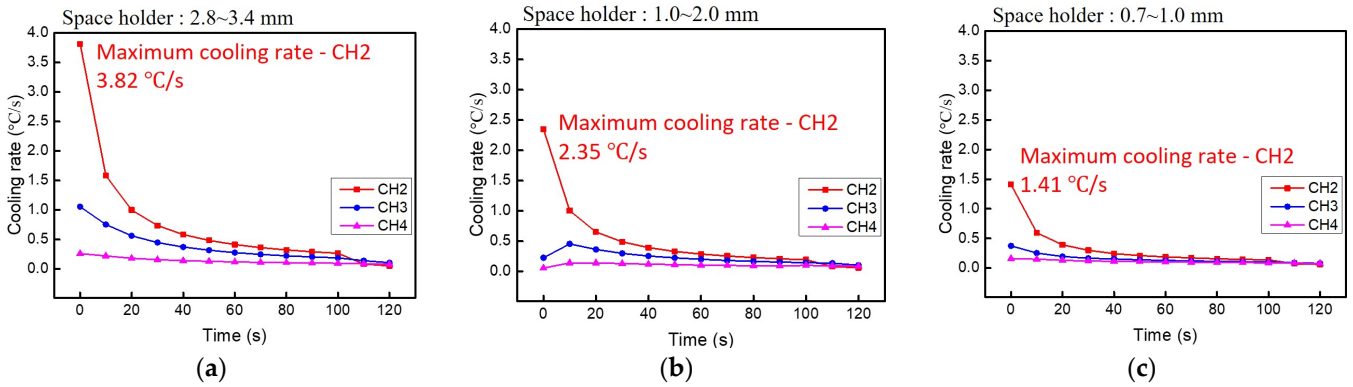

Figure 12. Cooling rate of the open-cell-type aluminum foams (five rammings) for the first 2 min while cooling by air-cooling system—100 LPM: (**a**) 2.8~3.4 mm space holder; (**b**) 1.0~2.0 mm space holder; (**c**) 0.7~1.0 mm space.

d_p is the diameter of the pore, and π is the porosity of the foam. As a result, as the pore size decreases to 2.8~3.4 mm, 1.0~2.0 mm, and 0.7~1.0 mm, the specific surface area per unit volume increases. This implies an increase in the surface area of the pores within the foams that can come in contact with the airflow. Commonly, a larger surface area leads to improved heat transfer efficiency. However, the experimental results in this work observed a contrary trend. Despite the increase in the specific surface area of the foams as the pore size decreases, the measured maximum cooling rate significantly decreases. As confirmed in Sections 3.2 and 3.3, when the pore size decreases, the flow of air becomes more complex due to an increase in the number of pores and a decrease in cell thickness, leading to an increase in pressure drop ΔP. For instance, under conditions with a porosity of approximately 62%, the foam with a pore size of 2.8~3.4 mm showed a pressure drop ΔP of 61 mbar, while for a pore size of 0.7~1.0 mm, the pressure drop ΔP increased to 108 mbar, representing an approximately 77% increase. Consequently, despite the increase in specific surface area, a decrease in pore size leads to higher pressure drop ΔP and lower air permeability, resulting in a degradation of cooling performance. This demonstrates that the heat-dissipation ability is dominated by the flow of air through the interconnected pores in foams. These results are similar to the research of Stefano Guarino et al. [37]. Their findings reported an increase in heat transfer efficiency as the airflow velocity increased. However, the limitation of their study is that it was restricted to conditions with the porosity of open-cell-type aluminum foams for over 95%, and they did not consider variations in porosity.

The cooling performance of the open-cell-type aluminum foams was evaluated by varying the porosity under the condition of similar porosity in this work. Through Figures 12 and 13, the cooling rates of the foams during the first 2 min with an airflow of 100 LPM were compared according to the ramming counts. It was measured that when the ramming counts were five, the porosity was about 62%, and when the ramming counts were two, the porosity was about 55% in Section 3.1. Under the foam with a pore size of 2.8~3.4 mm, as the porosity increased from 55% to 62%, the maximum cooling rate in-

creased by approximately 7.6%, from 3.55 °C/s to 3.82 °C/s. In the case of 1.0~2.0 mm pore size, the increase was 6.3%, and for 0.7~1.0 mm pore size, it was 2.2%. In open-cell-type aluminum foams with the same pore size, an increase in porosity leads to a decrease in average cell thickness, resulting in reduced pressure drop ΔP and improved air permeability. The flow of air through interconnected pores dominantly influences the cooling performance, and as shown in Equation (3), the specific surface area per unit volume increases with an increase in porosity. This aligns with the enhancement in heat dissipation in the foams with an increase in porosity. In the results of Section 3.2, while the variation in pressure drop ΔP due to changes in pore size was significant, exceeding 70%, the difference in pressure drop ΔP was only about 15% as increasing porosity from 55% to 62%. Considering these results, it was confirmed that the heat-dissipation ability of open-cell-type aluminum foams is greatly influenced by the variation in the pressure drop ΔP and the flow rate of air due to changes in pore size rather than porosity changes.

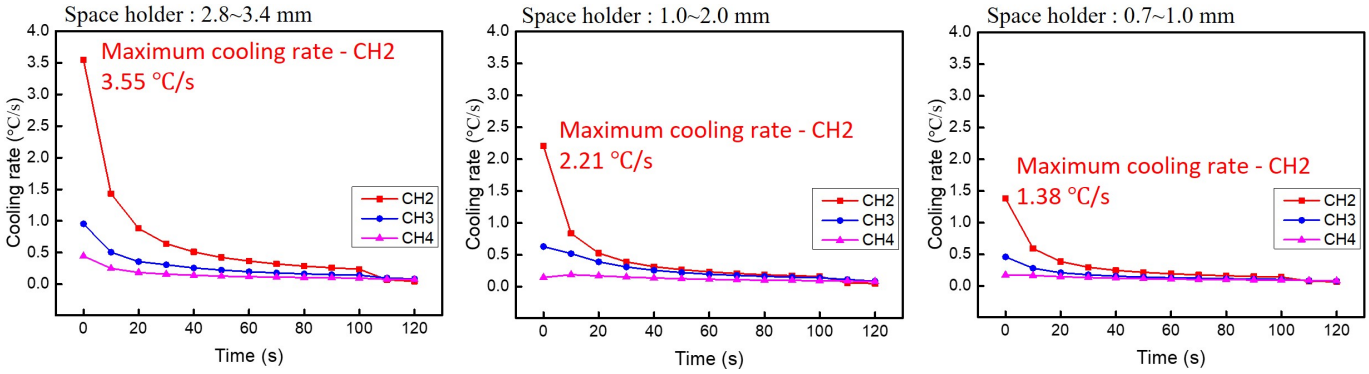

Figure 13. Cooling rate of the open-cell-type aluminum foams (two rammings) for the first 2 min while cooling by air-cooling system—100 LPM: (**a**) 2.8~3.4 mm space holder; (**b**) 1.0~2.0 mm space holder; (**c**) 0.7~1.0 mm space.

The cooling performance of open-cell-type aluminum foams is very high in the initial when forced convection within interconnected pores is induced. In particular, the difference in cooling rate from 0 to 1 min is substantial compared to the cooling rate from 1 to 2 min. Therefore, the cooling rate from 0 to 1 min can be an indicator of the cooling performance of open-cell-type aluminum foams based on structural conditions. Accordingly, to compare the heat dissipation of the foams used in the work with all variables, Figures 14 and 15 show the average cooling rate of all the samples from 0 to 1 min with different pore sizes, porosities, and volumetric flow rates of air.

The solid symbols in Figures 14 and 15 represent the average cooling rate during 0 to 1 min of the samples with a porosity of about 62%, while the hollow symbols represent the average cooling rate of the sample with a porosity of about 55%. The gray area was represented for the purpose of distinguishing channels in Figure 14 and for distinguishing volumetric flow rates in Figure 15 for convenience. The average cooling rate increases as the pore size of the open-cell-type aluminum foams increases. This is attributed to the fact that, even with equivalent porosity, the pressure drop ΔP decreases as the pore size increases, resulting in better airflow.

When the foams have the same pore size, the pressure drop ΔP decreases as the porosity increases. It means that airflow can be better through the foams with higher porosity, leading to an increase in the average cooling rate. However, in the case of the foams with a pore size of 0.7~1.0 mm, the effect of increasing the cooling rate with higher porosity is insufficient, as shown in Figure 14. At a volumetric airflow rate of 100 LPM, with a pore size of 2.8~3.4 mm, the maximum cooling rate increased by 7.6% as the porosity increased from approximately 55% to 62%. However, for a pore size of 1.0~2.0 mm, it was only a 2.2% increase. This result indicates that in foams with complex structures in

which numerous cells and cell walls are intertwined (high pressure drop ΔP and low air permeability), the improvement in heat-dissipation efficiency through changes in porosity is minimal.

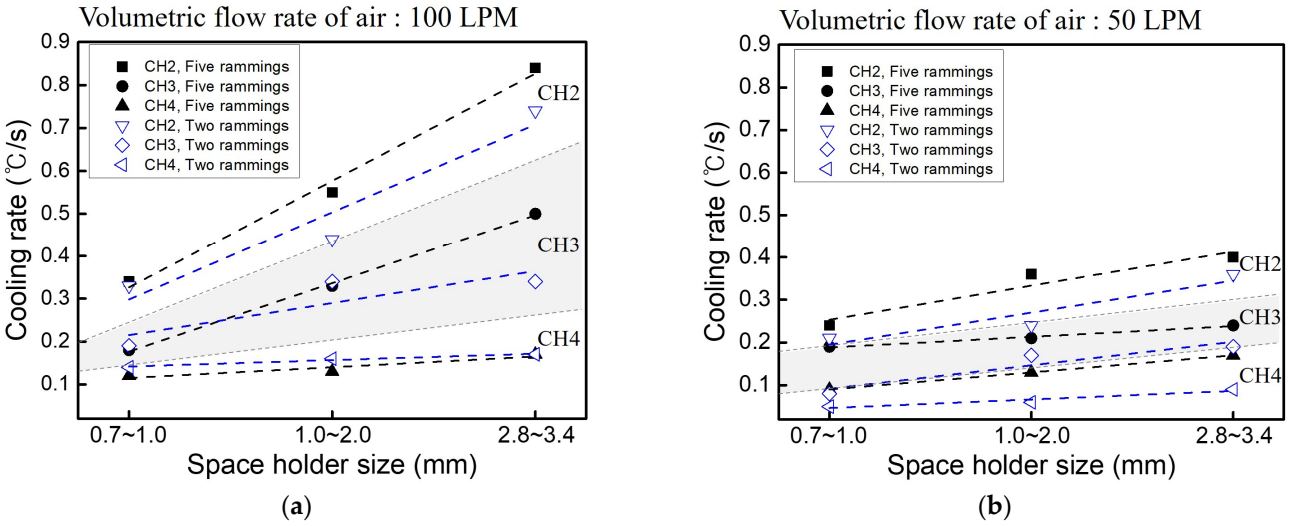

Figure 14. Average cooling rate of all the open-cell-type aluminum foams for the first 1 min: (**a**) 100 LPM; (**b**) 50 LPM. The gray area was represented for the purpose of distinguishing channels.

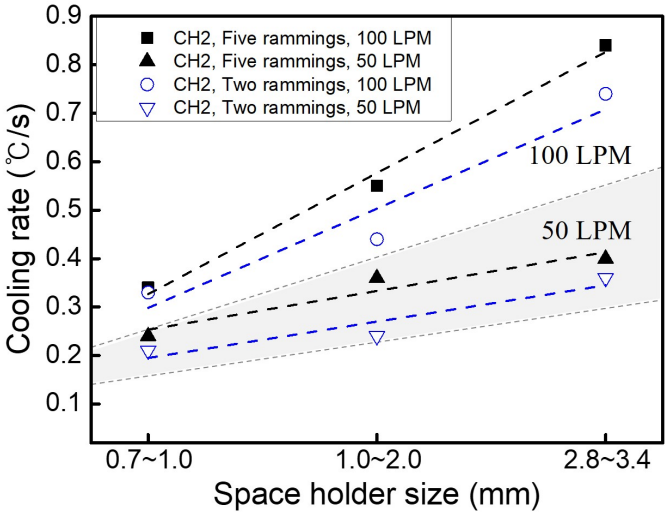

Figure 15. Average cooling rate of all the foams at CH2 for the first 1 min. The gray area was represented for distinguishing volumetric flow rates in Figure 15 for convenience.

Figure 15 illustrates the average cooling rate from 0 to 1 min at CH2 (the site closest to the air inlet) for all open-cell-type aluminum foams when the volumetric flow rate of air is 100 LPM and 50 LPM. It is confirmed that, under the same structural conditions of the foams, the average cooling rate increases as the volumetric flow rate of air increases. This is a natural result of the increase in the cooling energy source; however, for the foams with a pore size of 0.7~1.0 mm, there is no significant difference in the cooling rate despite increasing the amount of air injection. Promoting the cooling performance through structural conditions and volumetric flow rate is less effective for foams with small pore sizes. In other words, to improve the heat-dissipation ability of open-cell-type aluminum foams, it is advantageous to apply foams with large pore sizes and high porosity for a better flow rate.

For open-cell-type aluminum foams manufactured through the replication-casting process, it has been confirmed that the structural conditions significantly influence the

cooling performance and heat-dissipation efficiency of the foams using the air-cooling system. However, in this study, the effective thermal conductivity of the foams according to the structural conditions was not considered. Although various studies have reported the effective thermal conductivity of open-cell-type aluminum foams with changes in structural conditions [12,38–41], the trends observed in these studies do not align. The effective thermal conductivity of open-cell-type aluminum foams can affect the heat-dissipation ability of the foam. The device used in this experiment faces challenges in measuring the thermal conductivity of the foams. Therefore, we are contemplating the development of a device that can measure the effective thermal conductivity reflecting the structural conditions using the test samples employed in this experiment.

4. Conclusions

Through replication casting, which is a relatively simple process, the open-cell-type aluminum foams were successfully manufactured. The process allows for variations in pore size and porosity in foams by adjusting the size and stacking conditions of the space holder. The measured porosity of the foams ranged from approximately 55% to 62% based on the stacking conditions of the space holder, and the replicated pore sizes were 2.8~3.4 mm, 1.0~2.0 mm, and 0.7~1.0 mm, corresponding to the size of the space holder. The average cell thickness decreased as the pore size decreased under a similar porosity level, and under the same pore size, it decreased as the porosity increased.

The evaluation of thermal properties through the air-cooling system shows that the maximum cooling rate of the foams with 100 LPM was 3.82 °C/s to 1.41 °C/s under a porosity of about 62% and decreased significantly as the pore size decreased. When the same pore size, the maximum cooling rate increased by approximately 2.2% to 7.6% as the porosity increased from 55% to 62%. These variations in cooling performance are attributed to pressure drop ΔP and air permeability, and the flow of air through interconnected pores dominantly influences heat-dissipation ability over other factors. However, the small size of the pore (0.7~1.0 mm) causes an increase in resistance of airflow with intertwined structure, leading to minor improvement in heat-dissipation efficiency through changes in porosity. Consequently, the experimental results demonstrate that, for high-efficiency heat-dissipation ability, the rate of airflow through open-cell-type aluminum foams must be high, and this is more advantageous for foams with large pore sizes and high porosity.

Author Contributions: Conceptualization, J.K. and Y.K.; methodology, J.K.; validation, J.K. and Y.K.; data curation, J.K.; writing—original draft preparation, J.K., T.H., Y.L. and B.K.; writing—review and editing, J.K. and Y.K.; supervision, J.K. and Y.K.; formal analysis, T.H. and Y.L.; investigation, B.K. All authors have read and agreed to the published version of the manuscript.

Funding: This research received no external funding.

Data Availability Statement: The data presented in this study are available on request from the corresponding author (privacy).

Conflicts of Interest: The authors declare no conflicts of interest.

References

1. Zhang, J.; An, Y.; Ma, H. Research Progress in the Preparation of Aluminum Foam Composite Structures. *Metals* **2022**, *12*, 2047. [CrossRef]
2. García-Moreno, F. Commercial Applications of Metal Foams: Their Properties and Production. *Materials* **2016**, *9*, 85. [CrossRef] [PubMed]
3. Wan, T.; Liu, Y.; Zhou, C.; Chen, X.; Li, Y. Fabrication, Properties, and applications of open-cell aluminum foams: A review. *J. Mater. Sci. Technol* **2021**, *62*, 11–24. [CrossRef]
4. Dharmasena, K.P.; Wadley, H.N.G. Electrical Conductivity of Open-cell Metal Foams. *J. Mater. Res.* **2002**, *17*, 625–631. [CrossRef]
5. Monno, M.; Negri, D.; Mussi, V.; Aghaei, P.; Groppi, G.; Tronconi, E.; Strano, M. Cost-Efficient Aluminum Open-Cell Foams: Manufacture, Characterization, and Heat Transfer Measurements. *Adv. Eng. Mater.* **2018**, *20*, 1701032. [CrossRef]
6. Zhang, X.; Wang, R.; Li, X.; Lu, C.; Wang, Z.; Wang, W. Energy Absorption Performance of Open-Cell Aluminum Foam and Its Application in Landing Buffer System. *J. Mater. Eng. Perform.* **2021**, *30*, 6132–6145. [CrossRef]

7. Karuppasamy, R.; Barik, D. Production methods of aluminum foam: A brief review. *Mater. Today Proc.* **2021**, *37*, 1584–1587. [CrossRef]
8. Banhart, J. Aluminum foams for lighter vehicles. *Int. J. Veh. Des.* **2005**, *37*, 114–125. [CrossRef]
9. Banhart, J. Manufacture, characterization and application of cellular metals and metal foams. *Prog. Mater. Sci.* **2001**, *46*, 559–632. [CrossRef]
10. Hu, H.; Lai, Z.; Weng, X.; Ding, G.; Zhuang, D. Numerical model of dehumidifying process of wet air flow in open-cell metal foam. *Appl. Therm. Eng.* **2017**, *113*, 309–321. [CrossRef]
11. Hutter, C.; Büchi, D.; Zuber, V.; Rudolf von Rohr, P. Heat transfer in metal foams and designed porous media. *Chem. Eng. Sci.* **2011**, *66*, 3806–3814. [CrossRef]
12. Zhao, C.Y. Review on thermal transport in high porosity cellular metal foams with open cells. *Int. J. Heat Mass Transf.* **2012**, *55*, 3618–3632. [CrossRef]
13. Fischer, S.F.; Schüler, P.; Fleck, C.; Bührig-Polaczek, A. Influence of the casting and mould temperatures on the (micro)structure and compression behaviour of investment-cast open-pore aluminium foams. *Acta Mater.* **2013**, *61*, 5152–5161. [CrossRef]
14. Kulshreshtha, A.; Dhakad, S.K. Preparation of metal foam by different methods: A review. *Mater. Today-Proc.* **2019**, *26*, 1784–1790. [CrossRef]
15. Queheillalt, D.T.; Hass, D.D.; Sypeck, D.J.; Wadley, H.N.G. Synthesis of open-cell metal foams by templated directed vapor deposition. *J. Mater. Res.* **2001**, *16*, 1028–1036. [CrossRef]
16. Zhao, Y.Y.; Fung, T.; Zhang, L.P.; Zhang, F.L. Lost carbonate sintering process for manufacturing metal foams. *Scr. Mater.* **2005**, *52*, 295–298. [CrossRef]
17. Wan, T.; Liu, Y.; Zhou, C.; Ding, X.; Chen, X.; Li, Y. Fabrication of high-porosity open-cell aluminum foam via high-temperature deformation of $CaCl_2$ space-holders. *Mater. Lett.* **2021**, *284*, 129018. [CrossRef]
18. Neville, B.P.; Rabiei, A. Composite metal foams processed through powder metallurgy. *Mater. Des.* **2008**, *29*, 388–396. [CrossRef]
19. Sánchez, A.; Cruz, A.; Rivera, J.E.; Romero, J.A.; Suárez, M.A.; Gutiérrez, V.H. Manufacturing of Open-Cell Zn-22Al-2Cu Alloy Foams by a Centrifugal-Replication Process. *Metall. Mater. Trans. A* **2018**, *49*, 272–281. [CrossRef]
20. Dubinin, O.N.; Bondareva, J.V.; Kuzminova, Y.O.; Simonov, A.P.; Varfolomeev, I.A.; Yakimchuk, I.V.; Evlashin, S.A. A promising approach to 3D printing of metal foam with defined porosity. *J. Porous Mat.* **2023**, *30*, 1565–1573. [CrossRef]
21. Almonti, D.; Baiocco, G.; Tagliaferri, V.; Ucciardello, N. Design and Mechanical Characterization of Voronoi Structures Manufactured by Indirect Additive Manufacturing. *Materials* **2020**, *13*, 1085. [CrossRef]
22. Lu, T.J.; Stone, H.A.; Ashby, M.F. Heat transfer in open-cell metal foams. *Acta Mater.* **1998**, *46*, 3619–3635. [CrossRef]
23. Baloyo, J.M. Open-cell porous metals for thermal management applications: Fluid flow and heat transfer. *Mater. Sci. Technol.* **2017**, *33*, 265–276. [CrossRef]
24. Zhao, C.Y.; Lu, T.J.; Hodson, H.P.; Jackson, J.D. The temperature dependence of effective thermal conductivity of open-celled steel alloy foams. *Mater. Sci. Eng. A* **2004**, *367*, 123–131. [CrossRef]
25. Bracconi, M.; Ambrosetti, M.; Maestri, M.; Groppi, G.; Tronconi, E. A fundamental analysis of the influence of the geometrical properties on the effective thermal conductivity of open-cell foams. *Chem. Eng. Process.* **2018**, *129*, 181–189. [CrossRef]
26. Nie, Z.; Lin, Y.; Tong, Q. Numerical investigation of pressure drop and heat transfer through open cell foams with 3D Laguerre-Voronoi model. *Int. J. Heat Mass Transf.* **2017**, *113*, 819–839. [CrossRef]
27. Poureslami, P.; Siavashi, M.; Moghimi, H.; Hosseini, M. Pore-scale convection-conduction heat transfer and fluid flow in open-cell metal foams: A three-dimensional multiple-relaxation time lattice Boltzmann (MRT-LBM) solution. *Int. Commun. Heat Mass* **2021**, *126*, 105465. [CrossRef]
28. Calati, M.; de Monte, E.; Mancin, S. Numerical analysis of the effects of the structure shape and orientation of kelvin cell porous structures during air forced convection. *Appl. Sci.* **2021**, *11*, 6189. [CrossRef]
29. Zhu, W.; Kan, A.; Chen, Z.; Zhang, Q.; Zhang, J.; Yu, J.; He, Z. A modified Lattice Boltzmann method for predicting the effective thermal conductivity of open-cell foam materials. *Int. Commun. Heat Mass* **2022**, *133*, 105957. [CrossRef]
30. Zhang, C.; Kong, X.; Wang, X.; Du, Y.; Xiao, G. A Predicting Model for the Effective Thermal Conductivity of Anisotropic Open-Cell Foam. *Energies* **2022**, *15*, 6091. [CrossRef]
31. Kim, J.M.; Ha, T.K.; Han, B.S.; Kim, Y.J. Manufacturing Method and Thermal Properties of Open-Cell Type Aluminum Foam by Replication Casting Process. *Sol. State Phenom.* **2023**, *353*, 31–36. [CrossRef]
32. Lara-Rodriguez, G.A.; Figueroa, I.A.; Suarez, M.A.; Novelo-Peralta, O.; Alfonso, I.; Goodall, R. A replication-casting device for manufacturing open-cell Mg Foams. *J. Mater. Process. Tech.* **2017**, *243*, 16–22. [CrossRef]
33. Dairon, J.; Gaillard, Y.; Tissier, J.C.; Balloy, D.; Degallaix, G. Parts containing open-celled metal foam manufactured by the foundry route: Processes, performances, and applications. *Adv. Eng. Mater.* **2011**, *13*, 1066–1071. [CrossRef]
34. Yu, J.; Wu, Q.; Bu, L.; Nie, Z.; Wang, Y.; Zhang, J.; Zhang, K.; Renchen, N.; He, T.; He, Z. Experimental study on improving lithium extraction efficiency of salinity-gradient solar pond through sodium carbonate addition and agitation. *Sol. Energy* **2022**, *242*, 364–377. [CrossRef]
35. Richardson, J.T.; Peng, Y.; Remue, D. Properties of ceramic foam catalyst supports: Pressure drop. *Appl. Catal. A-Gen.* **2000**, *204*, 19–32. [CrossRef]
36. Liu, J.F.; Wu, W.T.; Chiu, W.C.; Hsieh, W.H. Measurement and correlation of friction characteristic of flow through foam matrixes. *Exp. Therm. Fluid Sci.* **2006**, *30*, 329–336. [CrossRef]

37. Guarino, S.; Rubino, G.; Tagliaferri, V.; Ucciardello, N. Thermal behavior of open cell aluminum foams in forced air: Experimental analysis. *Measurement* **2015**, *242*, 364–377. [CrossRef]
38. Wu, D.; Huang, C. Thermal conductivity model of open-cell foam suitable for wide span of porosities. *Int. J. Heat Mass Transf.* **2019**, *130*, 1075–1086. [CrossRef]
39. Babcsán, N.; Mészáros, I.; Hegman, N. Thermal and Electrical Conductivity Measurements on Aluminum Foams. *Mater. Werkst.* **2003**, *34*, 391–394. [CrossRef]
40. Pandey, A.; Dubey, R.; Jain, H.; Abhas, A.; Kumar, R.; Gupta, G.K.; Siram, S.; Chilla, V.; Mondal, D.P. Effect of cell size on the microarchitectural and physicomechanical response in open-cell Al foam made through template method. *Mater. Chem. Phys.* **2023**, *296*, 127341. [CrossRef]
41. Hernandez, J.N.C.; Link, G.; Schubert, M.; Hampel, U. Novel Mixing Relations for Determining the Effective Thermal Conductivity of Open-Cell Foams. *Materials* **2022**, *15*, 2168. [CrossRef] [PubMed]

Disclaimer/Publisher's Note: The statements, opinions and data contained in all publications are solely those of the individual author(s) and contributor(s) and not of MDPI and/or the editor(s). MDPI and/or the editor(s) disclaim responsibility for any injury to people or property resulting from any ideas, methods, instructions or products referred to in the content.